ICNMM2018-7658

Modeling of Flow Distribution in Proton Exchange Membrane Fuel Cell

Omid Babaie Rizvandi, Serhat Yesilyurt
Mechatronics Program, Sabanci University
Istanbul, Turkey

ABSTRACT

Analysis and design of flow fields for proton exchange membrane fuel cell (PEMFC) require coupled solution of the flow fields, gas transport and electrochemical reaction kinetics in the anode and the cathode. Computational cost prohibits the widespread use of three-dimensional models of the anode and cathode flow fields, gas diffusion layers (GDL), catalyst layers (CL) and the membrane for fluid flow and mass transport. On the other-hand, detailed cross-sectional two-dimensional models cannot resolve the effects of the anode and cathode flow field designs. Here, a two-dimensional in-plane model is developed for the resolution of the effects of anode and cathode flow channels and GDLs, catalyst layers are treated as thin-layers of reaction interfaces and the membrane is considered as a thin-layer that resist the transfer of species and the ionic current. Brinkman equations are used to model the in-plane flow distribution in the channels and the GDLs to account for the momentum transport in the channels and the porous GDLs. Fick's law equations are used to model transport of gas species in the channels and GDLs by advection and diffusion mechanisms, and electrochemical reactions in the CL interfaces are modeled by Butler-Volmer equations. Complete features of the flow in the channels and inlet and outlet manifolds are included in the model using resistance relationships in the through-plane direction. The model is applied to a small cell having an active area of 1.3 cm^2 and consisting of 8 parallel channels in the anode and a double serpentine in the cathode. Effects of the anode and cathode stoichiometric ratios on the cell performance and hydrogen utilization are investigated. Results demonstrate that for a sufficiently high cathode stoichiometric ratio enough, anode stoichiometric ratio can be lowered to unity to obtain very high hydrogen utilization and output power.

1. NOMENCLATURE

Abbreviation

CL	Catalyst layer
CFD	Computational fluid dynamics
DOF	Number of degree of freedom
GDL	Gas diffusion layer
PEMFC	Proton exchange membrane fuel cell
rms	Root-mean-square
St	Stoichiometric ratio

Symbols

a	Water activity
c	Concentration
D	Diffusion coefficient
F	Faraday's factor
J	Current density
K	Permeability
L	Length
n_d	Electro-osmatic drag coefficient
p	pressure
R	Universal gas constant
R_{solid}	Electric resistance of the cell components
S	Source term
T	Temperature
$\mathbf{u}$	Velocity vector
v	Molar volume
w	Width, mass fraction
x	Molar fraction

Greek letters

∇	Vector differential operator
δ	Thickness
ρ	Density
σ	Electric conductivity
μ	Dynamic viscosity
ε	Porosity
α	Charge transfer coefficient
ψ	Permeance coefficient
γ	Concentration coefficient
λ	Water content

2. INTRODUCTION

Proton exchange membrane fuel cell (PEMFC), also known as polymer electrolyte membrane fuel cell, is a promising energy conversion device that can be used in the stationary and portable applications. The main advantages of PEMFC are high efficiency (almost twice the conventional internal combustion

engines), high power density, fast start-up time, low operating temperature (less than 80 °C), and low emission. However, disadvantages such as high cost due to cost of the platinum as catalyst material and hydrogen storage, and degradation issues are barriers against their commercialization [1-4].

A complete model of the PEMFC consists of multi-physics interactions such as flow, species transport, electrochemical reactions, phase change, heat transfer, and structural mechanics. To attain a reasonable computational time, for the expanse of accuracy and geometric complexity lower-dimensionality models are preferred, while more assumptions and simplifications are used for higher-dimensionality models. Karvonen et al. [5] developed two and three-dimensional models to investigate a uniform flow distribution in parallel channels used for the cathode side to enhance the cell performance. Authors reported that mesh for the 3D model consists of 180K elements and 1.2M degrees of freedom (DOF) for a 12 by12.6 cm flow field. Rostami et al. [6] developed a three dimensional model to investigate the effect of the bend size of a serpentine flow field on the performance of the PEMFC. They performed a grid independence test and found that for the channels with square bend size of 1.2 mm about 500 K cells are required. Hu et al. [7] employed a three-dimensional model to investigate the effects of the interdigitated and conventional flow fields on the cell performance. They utilized about 400 K grid size to mesh a single channel with the length and width of 6 and 0.07 cm and half of ribs at each side of the channel used for the anode and cathode sides, and components between them. Vazifeshenas et al. [8] developed a three-dimensional CFD model to compare the effect of the parallel, serpentine, and compound flow fields on the PEMFC performance. According to their results, 690K elements are needed for mesh independent results for a flow field of 5 by 5 cm. In this study, the grid size and DOF are reduced significantly by developing a 2D in-plane model with resistance relationships used for the through-plane direction and complete details are kept for the flow channels and inlet and outlet manifolds in the anode and the cathode.

Evaluating the exact flow distribution in a porous medium by solving Navier-Stokes equations is difficult as it is based on the definition of the geometry of the complex porous structure [9,10]. Darcy's law, which uses volume-averaged quantities, is the standard approach for the flow in a porous medium. Whitaker [11] applied volume averages to the Stokes momentum equation and obtained a more general equation than the Darcy's law and similar to the form proposed by Brinkman [12]. In addition to the terms in the Darcy's law, Brinkman equation contains an extra source term that represents the drag force of the fluid at the boundaries of the solid phase of the porous medium and the walls of the domain. Darcy's law is used to model flow fields in the GDL and CL because of its simplicity [13,14]; however its accuracy is less than Brinkman and Navier-Stokes equations. Shi and Wang [15] applied Darcy's law, Brinkman equation, modified Navier-Stokes, and pure diffusion equation to the anode and cathode electrodes (GDLs and CLs). They reported that using Brinkman equation can improve the bounda-

ry condition problems of Darcy's law, and the convergence problems arise from the modified Navier-Stokes equation. Brinkman equation is solved in the porous medium instead of Darcy's law in many recent models [16,17].

This paper concerns a two-dimensional, single-phase, in-plane, and isothermal model of the anode and cathode flow fields and GDLs of a PEMFC. Brinkman equation is used to model flow distribution in the channels and the GDLs, and it is coupled to the mass transfer of species along and across the flow field by advection and diffusion mechanisms, Fick's law, and reactions kinetics, Butler-Volmer, equations. Anode and cathode sides are coupled with the resistance relations in the through-plane direction. First, the polarization curve from the model is validated against the polarization curve reported by Ye & Van Nguyen [18]. Moreover, the effects of the anode and cathode stoichiometric ratios on the cell performance, hydrogen utilization, and species distribution in the flow fields are investigated.

3. METHODOLOGY

A two-dimensional model of the anode and cathode flow fields and GDLs is developed. Modeling both anode and cathode channels and GDLs in 2D in-plane by projecting them on a single surface is demonstrated in Fig. 1. Anode and cathode flow fields consisting of 8 parallel and double serpentine channels, respectively, are shown in Fig. 2. With the overlapping partitions of the active area in this 2D representation, multiple equations are solved in each domain and the through plane interactions are reduced to resistance relationships between the variables representing different regions in the third dimension.
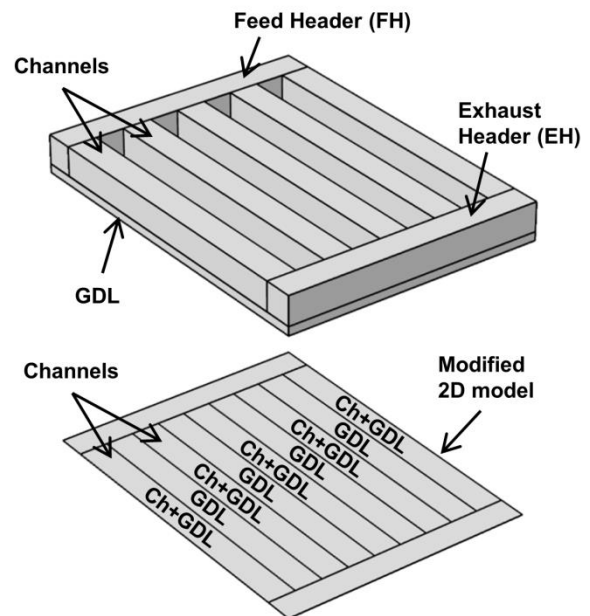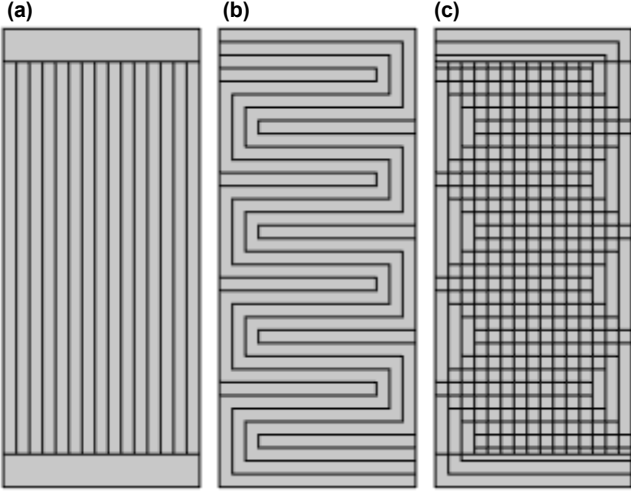

FIGURE 1: Flow field schematic, 3D (top) and modified 2D (bottom)

FIGURE 2: Flow fields: (a) anode, (b) cathode, (c) anode and cathode on the same plane

3.1. Governing equations

Brinkman equations are used to model the flow distribution in the flow fields and GDLs, Fick's law to model species transport through the membrane and in the flow field resulting from both diffusion and advection mechanisms, and Butler-Volmer equations to determine electrochemical reactions kinetics at the anode and cathode CLs. These models are coupled and solved simultaneously to achieve a comprehensive model that describes the flow distribution, transport of species, and the cell voltage. Values of the parameters used in this model are listed in Table 1.

3.1.1. Fluid flow

Brinkman equations, which are more generalized than Darcy's law [19,20], take care of both stress and fluid transfer at the boundaries of the void medium, channel, and the porous GDLs, by including viscous momentum transfer at the interfaces between solid and pore domains that the porous and non-porous fluid regions are coupled easily. Therefore, heterogeneous domains can be represented easily in two-dimensions.

Brinkman momentum and mass conservation equations are:

$$\rho \mathbf{u} \cdot \nabla \mathbf{u} = -\nabla p + \mu \nabla^2 \mathbf{u} - \frac{\mu}{K} \mathbf{u} \tag{1}$$

$$\nabla \cdot (\rho \mathbf{u}) = S_{br} \tag{2}$$

where p is the pressure, $\mathbf{u}$ the velocity vector, μ the dynamic viscosity, K the permeability of the porous region, and S_{br} is the mass source which is from the reactions of hydrogen and oxygen at the CLs and transfer of nitrogen and water vapor across the membrane. The last term in the right-hand-side of Eq. (1) is from the Darcy's law which is due to the viscous friction of the fluid at the boundaries of the solid phase of the domain. Porosity and permeability of the channel are determined based on the Hele-Shaw relation which is used for a viscous flow between

Table 1: Parameters and their values used in the model

Parameter	Value	Description
δ_m	50×10^{-6} m	Thickness of the membrane
δ_{GDL}	3×10^{-4} m	Thickness of the GDL
L	0.015 m	Length of the channels
w_{ch}	5×10^{-4} m	Width of the channels
w_{rib}	5×10^{-4} m	Width of the ribs
F	96,485 C/mol	Faraday's constant
T, T_{ref}	343 and 298 K	Operation and reference temperatures
P, P_0	1.5 and 1 atm	Operation and reference pressures
K_{GDL}	3×10^{-12} m^2	Permeability of the GDL
ε_{GDL}	0.7	Porosity of the GDL
R_{solid}	10^{-5} Ω	Electric resistance of the components of the cell
V_m	9×10^{-4} m^3/mol	Molar volume of the membrane
v_{H_2}	7.07×10^{-6} m^3/mol	Molar volume of hydrogen
v_{N_2}	17.9×10^{-6} m^3/mol	Molar volume of nitrogen
$c_{SO_3}^0$	1.2×10^3 mol/m^3	Concentration of sulfonic in the membrane
$\psi_{N_2,0}$	10^{-14} mol/m^2	Reference permeance coefficient of N_2
$i_{0,ref,343K}^{(an,ca)}$	1×10^4 and 7×10^{-2} A/m^2	Reference current density at the anode and cathode at 343 K, [18]
$J_{loss,0}$	20 A/m^2	Parasitic current density
$\gamma_{\{H_2,O_2\}}$	0.5 and 1	Concentration coefficients of H_2 and O_2
$\alpha_{\{an,ca\}}$	1 and 1	Charge transfer coefficient for the anodic and cathodic reactions

two parallel plates at a small distance [21]:

$$K_{ch} = \frac{h^2}{12} \tag{3}$$

$$\varepsilon_{ch} = 1$$

Here, h is the height of the channel. Brinkman equations impose the mass and momentum transfer between the channels and GDL by means of this artificial permeability used for the channel and the GDL permeability, and the porosities of the channels and GDL.

Brinkman equation is solved over the flow fields to determine the velocity distribution in the channels and GDLs. A constant flow rate based on the stoichiometric ratio of the anode and cathode sides at a reference current density, 1 A/cm^2, is specified at the inlets, 1.5 atm pressure is set to the outlets, and no-slip boundary condition is used at the walls of the anode and cathode flow fields.

3.1.2. Mass transfer

Advection and diffusion transport of species in the flow fields developed by Brinkman equations and across the membrane is determined by Fick's law [22]:

$$\nabla \cdot \left(-\rho D_i \nabla w_i + \rho w_i \mathbf{u} \right) = S_i \tag{4}$$

where w is the mass fraction, ρ the density, D the diffusion coefficient, $\mathbf{u}$ the convective velocity form the Brinkman equation, S the reaction rate, and i denotes the species, which are hydrogen and water vapor in the anode, and oxygen, nitrogen and water vapor in the cathode. One of the species on each side can be obtained from the conservation law:

$$\sum w_i = 1 \tag{5}$$

Diffusion coefficient of the hydrogen and water vapor at the anode side, and oxygen, water vapor, and nitrogen at the cathode side are given by [18]:

$$D_{H_2}^{an} = D_{H_2O}^{an} = 1.055 \times 10^{-4} \left(\frac{T}{333} \right)^{1.75} \left(\frac{101325}{p} \right)$$

$$D_{H_2O}^{ca} = 0.2982 \times 10^{-4} \left(\frac{T}{333} \right)^{1.75} \left(\frac{101325}{p} \right) \tag{6}$$

$$D_{O_2}^{ca} = D_{N_2}^{ca} = 0.2652 \times 10^{-4} \left(\frac{T}{333} \right)^{1.75} \left(\frac{101325}{p} \right)$$

Here, T and p are operation temperature and pressure, respectively. Bruggeman correction is used to determine diffusion coefficients of the species in GDL based on their values in the channels [23]:

$$D_{ij}^{GDL} = D_{ij}^{ch} \varepsilon^{1.5} \tag{7}$$

where ε is the porosity.

Through-plane flux of hydrogen that takes part in the reaction at the anode CL is given by:

$$N_{H_2}^{an} = -\frac{M_{H_2}}{2F} \left(J_{cell} + J_{loss} \right) \tag{8}$$

Here, F is Faraday's constant, J_{cell} the current density, and J_{loss} the parasitic current density due to the loss of hydrogen diffusion to the cathode side and defined as a function of the mole fraction of hydrogen:

$$J_{loss} = J_{loss,0} x_{H_2} \tag{9}$$

where $J_{loss,0}$ is a constant determined from the permeance of hydrogen through the membrane.

Inward flux of the water vapor to the anode side is a function of current density and membrane water content at the anode and cathode CLs:

$$N_{H_2O}^{an} = M_{H_2O} \left[\frac{c_{SO_3}^0 \left(\lambda_{ca} - \lambda_{an} \right)}{R_m} - n_d \frac{J_{cell}}{F} \right] \tag{10}$$

Here, $c_{SO_3}^0$ is the concentration of sulfonic in the dry membrane, n_d the electro-osmotic drag coefficient, R_m the resistance to the water transport across the membrane, and $\lambda_{an/ca}$ the water content at the anode and cathode CLs which is determined by:

$$\lambda_i = \begin{cases} 1.41 + 11.3 a_i - 18.8 a_i^2 + 16.2 a_i^3 & 0 \le a_i \le 1 \\ 10.1 + 2.94 \left(a_i - 1 \right) & 1 < a_i \le 3 \\ 16 & 3 < a_i \end{cases} \tag{11}$$

where a is the water activity:

$$a = x_{H_2O} \frac{P}{P_{sat}} \tag{12}$$

where P_{sat} is the saturation pressure of water at the operation temperature. Resistance to the water transport across the membrane is defined as:

$$R_m = \frac{1}{k_{ads}} + \frac{1}{k_{des}} + \frac{\delta_m}{D_\lambda} \tag{13}$$

Here, k_{ads} and k_{des} are the adsorption and desorption coefficients, and D_λ the diffusion coefficient of water in the membrane. Adsorption and desorption coefficients are given by [24]:

$$k_{ads} = 1.14 \times 10^{-5} f_v \exp \left[2416 \left(\frac{1}{T} - \frac{1}{T_0} \right) \right]$$

$$k_{des} = 4.59 \times 10^{-5} f_v \exp \left[2416 \left(\frac{1}{T} - \frac{1}{T_0} \right) \right] \tag{14}$$

where f_v is the volumetric ratio of the liquid water in the membrane and determined by:

$$f_V = \frac{\lambda V_{H_2O}}{V_m + V_{H_2O}} \tag{15}$$

where λ is the membrane water content which is defined as the molar ratio of water molecules per sulfonic group in the membrane, V_{H_2O} and V_m are the molar volumes of the liquid water and dry membrane, respectively. Membrane water content is defined as the mean of the equilibrium water contents at the anode and cathode sides:

$$\lambda = \frac{\lambda_{an} + \lambda_{ca}}{2} \tag{16}$$

Diffusion coefficient of the water in the membrane is determined by [25]:

$$D_\lambda = \begin{cases} D_{\lambda,0} \left(2.05 D_{\lambda,0} - 3.25 \right) & 2 < \lambda \le 3 \\ D_{\lambda,0} \left(6.65 - 1.25\lambda \right) & 3 < \lambda \le 4 \\ D_{\lambda,0} \left(2.563 - 0.33\lambda + & 4 < \lambda \\ \quad 2.64 \times 10^{-2} \lambda^2 - 6.71 \times 10^{-4} \lambda^3 \right) \end{cases} \tag{17}$$

$$D_{\lambda,0} = 10^{-10} \exp \left[2416 \left(\frac{1}{T_{ref}} - \frac{1}{T} \right) \right]$$

Flux of the oxygen that takes part in the reaction at the cathode catalyst layer is determined by:

$$N_{O_2}^{ca} = -\frac{M_{O_2}}{4F} \left(J_{cell} + J_{loss} \right) \tag{18}$$

4

Flux of the generated water at the cathode side is defined as:

$$N_{H_2O,gen}^{ca} = \frac{M_{H_2O}}{2F}\left(J_{cell} + J_{loss}\right) \qquad (19)$$

Flux of water vapor from the cathode to the anode is determined from the generated water at the cathode side and inward flux of the water vapor to the anode side:

$$N_{H_2O}^{ca} = N_{H_2O,gen}^{ca} - N_{H_2O}^{an} \qquad (20)$$

The right hand side of the Fick's law equation, the source term in Eq. (4), is the reaction rate of species. Reactions of the species at the catalyst layers are defined based on their fluxes in the through-the-plane direction:

$$S_i = \frac{N_i}{d_{eff}} \qquad (21)$$

where d_{eff} is the effective depth of the channels and GDLs:

$$d_{eff} = \frac{V_{Total}}{A_{active}} \Rightarrow \begin{cases} d_{eff,ch} = h_{ch} + h_{GDL}\varepsilon \\ d_{eff,GDL} = h_{GDL}\varepsilon \end{cases} \qquad (22)$$

Here, V_{Total} is the total volume available to the species in the channel or GDL, A_{active} the active area, h_{ch} the channel height, and h_{GDL} the GDL height.

3.1.3. Reactions kinetics

To model potential distribution in the cell, conservation of charge is applied to the electrolyte and electrodes:

$$\begin{aligned} \sigma_e \nabla \phi_e &= 0 \\ \sigma_s \nabla \phi_s &= 0 \end{aligned} \qquad (23)$$

where σ and ϕ are the electric conductivity and potential, respectively, and subscripts e and s denote electrolyte and electrodes, respectively. Anode electrode is chosen as the ground electrode and cathode electrode potential is the sum of the reversible cell potential, V_{rev}, activation overpotentials, ΔV_{an} and ΔV_{ca}, and ionic and ohmic potential drops, ΔV_m and ΔV_{ohm}, as follows:

$$V_{cell} = V_{rev} - \Delta V_m - \Delta V_{ohm} - \Delta V_{an} - \Delta V_{ca} \qquad (24)$$

The reversible cell potential is given by [26]:

$$V_{rev} = V_0 - \frac{RT}{2F} \ln\left[\frac{a_{H_2O}}{a_{H_2}\sqrt{a_{O_2}}}\right] \qquad (25)$$

where a_i is the ratio of the pressure of species i to the operation pressure, and V_0 is the open-circuit potential and given by [27]:

$$V_0 = 1.23 - 0.00083 \times \left(T - T_{ref}\right) \qquad (26)$$

Resistance of the membrane against ionic current leads to ionic potential drop which is a function of membrane water content, temperature, and current density. Ionic conductivity of the membrane is approximated linear over the membrane based on its value at the anode and cathode CLs:

$$\sigma_m = \frac{\sigma_m^{ca} - \sigma_m^{an}}{\delta_m}x + \sigma_m^{an} \qquad (27)$$

where, σ_m is the ionic conductivity of the membrane, and superscripts ca and an denote the corresponding values at the cathode and anode CLs, respectively. Membrane ionic conductivity in the CLs is given by [18]:

$$\sigma_m^{an,ca} = \left(-0.326 + 0.514\lambda^{an,ca}\right)\exp\left[1268\left(\frac{1}{303} - \frac{1}{T}\right)\right] \qquad (28)$$

and ionic potential loss is defined as:

$$\Delta V_m = \int_0^{\delta_m} \frac{J_{cell}}{\sigma_m}dx = \frac{\delta_m J_{cell}}{\sigma_m^{ca} - \sigma_m^{an}}\ln\left(\frac{\sigma_m^{ca} - \sigma_m^{an}}{\sigma_m^{an}} + 1\right) \qquad (29)$$

Resistance of the cell components against the movement of electrons results in the ohmic potential loss:

$$\Delta V_{ohm} = R_{solid}J_{cell} \qquad (30)$$

Here, R_{solid} is the total electric resistance of the solid components of the cell which is estimated from the slope of the polarization curve of the experiments.

Anode and cathode activation overpotentials can be determined by applying a concentration modified form of the Butler-Volmer equation to the anode and cathode sides and solve the system of equations for the overpotentials:

$$\Delta V_{an,ca} = \frac{RT}{F\alpha_{an,ca}}a\sinh\left[\frac{J_{cell}}{i_{0,ref}^{an,ca}}\left(\frac{c_{H_2,O_2}^{ref}}{c_{H_2,O_2}^{CL}}\right)^{\gamma_{H_2,O_2}}\right] \qquad (31)$$

where α is the charge transfer coefficient of the anodic and cathodic reactions, γ the concentration coefficient, $i_{0,ref}$ the reference current density, and c_i^{CL} the concentration of species i in the catalyst layer, which is calculated from the resistance model in the GDL:

$$c_i^{CL} = c_i - \frac{\delta_{GDL}}{D_{i,N_2}}N_i \qquad (32)$$

where δ_{GDL} is the thickness of the GDL, D_{i,N_2} the binary diffusion coefficient of species i and nitrogen, and N_i the mass flux of species i. The reference current density is a function of temperature and defined based on its value at 343 K [18]:

$$i_{0,ref} = i_{0,ref,343K}\exp\left[\frac{6.6\times10^4}{R}\left(\frac{1}{343} - \frac{1}{T}\right)\right] \qquad (33)$$

The unknowns are the velocity field, molar fraction of hydrogen at the anode side, molar fractions of oxygen and water vapor at the cathode side, and the cell potential. These unknowns are calculated by coupling and solving all above mentioned equations.

3.2. Numerical approach

Brinkman, Fick's law, and Butler-Volmer equations are coupled and solved numerically over the anode and cathode
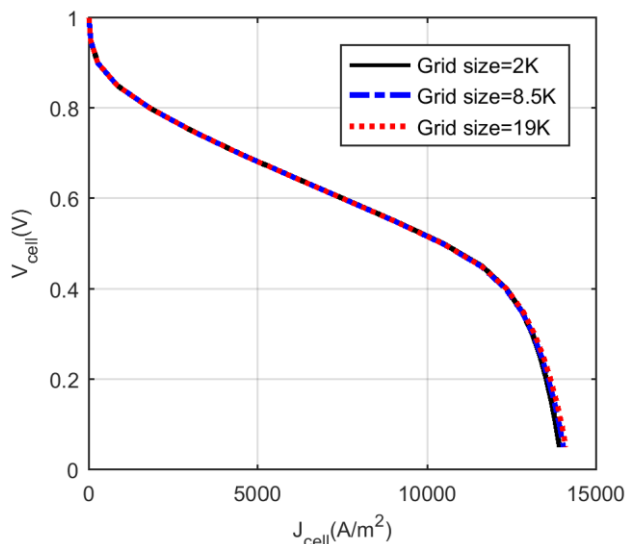
FIGURE 3: Grid convergence study of the model

flow fields by the commercial finite element package, COM-SOL Multiphysics.

Quadrangular mesh is used to discretize the modeling domain. To certify the accuracy of the numerical results, a grid convergence study is carried out. Polarization curves obtained from the model with the stoichiometric ratios of 3 and 1 for the cathode and anode sides, respectively, are compared for different grid sizes, as shown in Fig. 3. The minimum grid size that can be used to mesh the model geometry is about 2 K. Figure 3 shows the polarization curves for the grid size of 2, 8.5, and 19 K. The difference between the polarization curves is negligible. Therefore, the grid size of 2 K is chosen which results in the number of degree of freedom (DOF) of 48 K. Fully-coupled solver using Newton iterations with relative tolerance of 10^{-3} and direct MUMPS is employed to solve the linear system of equations.

4. RESULTS

In order to verify the developed model, the polarization curve obtained from the model is compared to the one reported by Ye & Van Nguyen [18]. Moreover, effect of the anode and cathode stoichiometric ratios on the cell performance, hydrogen utilization, and species distribution in the flow field are investigated.

4.1. Model validation

Accuracy of the model developed in this study is examined by validating the polarization curve obtained from the model with single phase assumption against the polarization curve reported by Ye & Van Nguyen [18]. Figure 4a shows the representation of the reduction of the 3D model to 2D in-plane model. Here, channels and GDLs are placed on a single plane and CLs and membrane are treated as thin layers. In addition to the geometry, physical model and parameters reported by Ye & Van
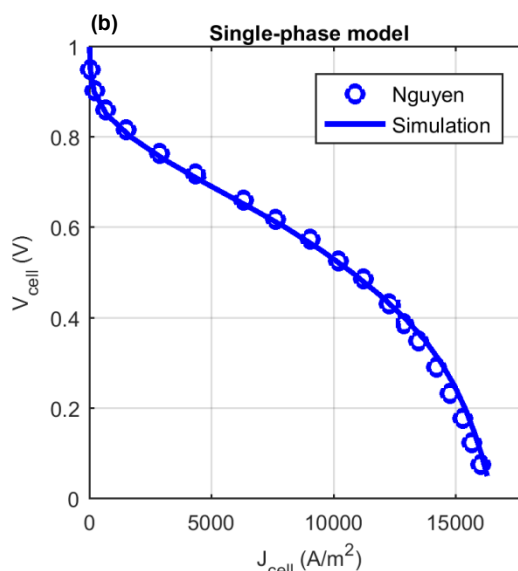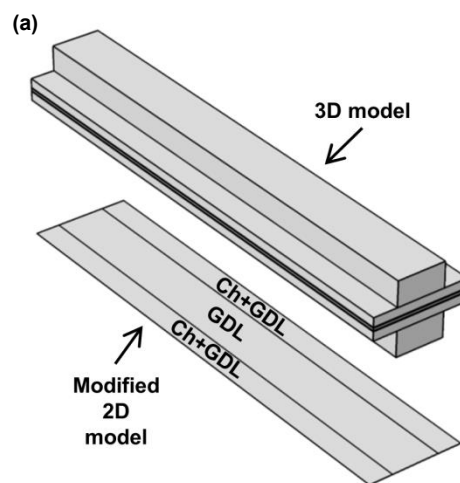

FIGURE 4: Validation of the model: a) schematic of 3D, [18], and 2D, this study, modeling domains, b) comparison of the polarization curve obtained from the current model and the one reported by Ye & Van Nguyen [18] for the single phase model

Nguyen [18] for the single phase model are applied to the 2D model and the polarization curves are compared, as demonstrated in Fig. 4b with very good agreement between the polarization curves. The maximum error between the cell potentials is 36 mV at Jcell = 15600 A/m^2.

4.2. Species distribution

Stoichiometric ratio plays an important role on the cell performance and defined as the ratio of reacting amount of species to the amount supplied from the inlet for hydrogen in the anode and oxygen in the cathode. Typically, cathode stoichiometric ratio must be significantly larger than unity due to slow kinetics
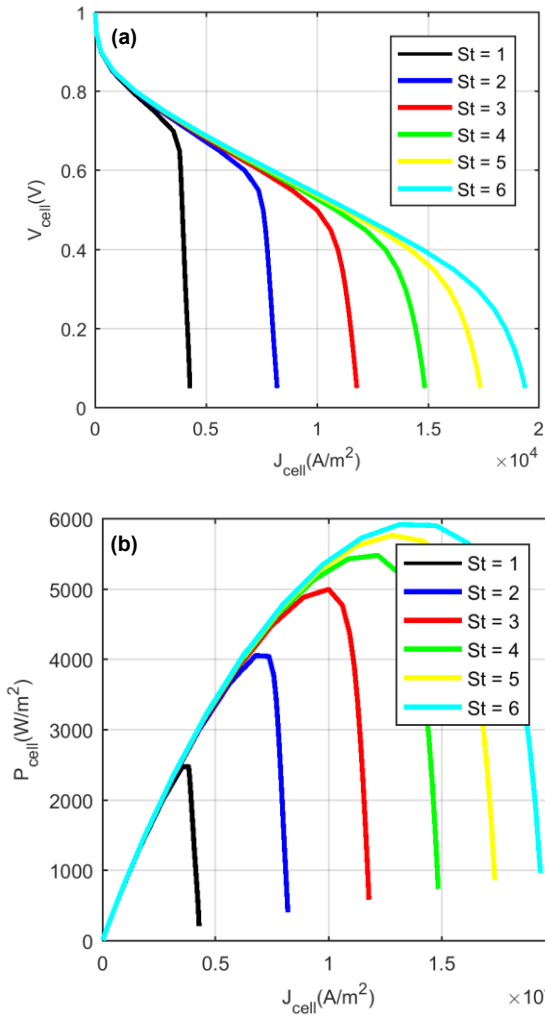
FIGURE 5: Effect of the stoichiometric ratio on the cell performance: a) polarization curve; b) power curve; anode and cathode stoichiometric ratios are considered equal

of the cathode reaction, whereas the anode stoichiometric ratio can be kept close to unity due to fast kinetics. Inlet flow rates are specified based on the stoichiometric ratios at a reference current density, which is 1 A/cm^2 in this study. Figures 5a and 5b show the effect of the stoichiometric ratio, which is kept the same in the anode and cathode sides, on the cell performance, polarization and output power density. Higher stoichiometric ratio results in higher output power as demonstrated in Fig. 5b, but lower hydrogen utilization, which is an important performance metric in the operation of PEMFC, especially at low current densities.

Figure 6a shows that the output power is the same for different anode stoichiometric ratios if the cathode stoichiometric ratio is fixed to 3. However, hydrogen utilization is enhanced for lower anode stoichiometric ratio, as indicated in Fig. 6b. A common problem in utilizing low stoichiometric ratio condition for the anode side is the flow maldistribution, [28], which
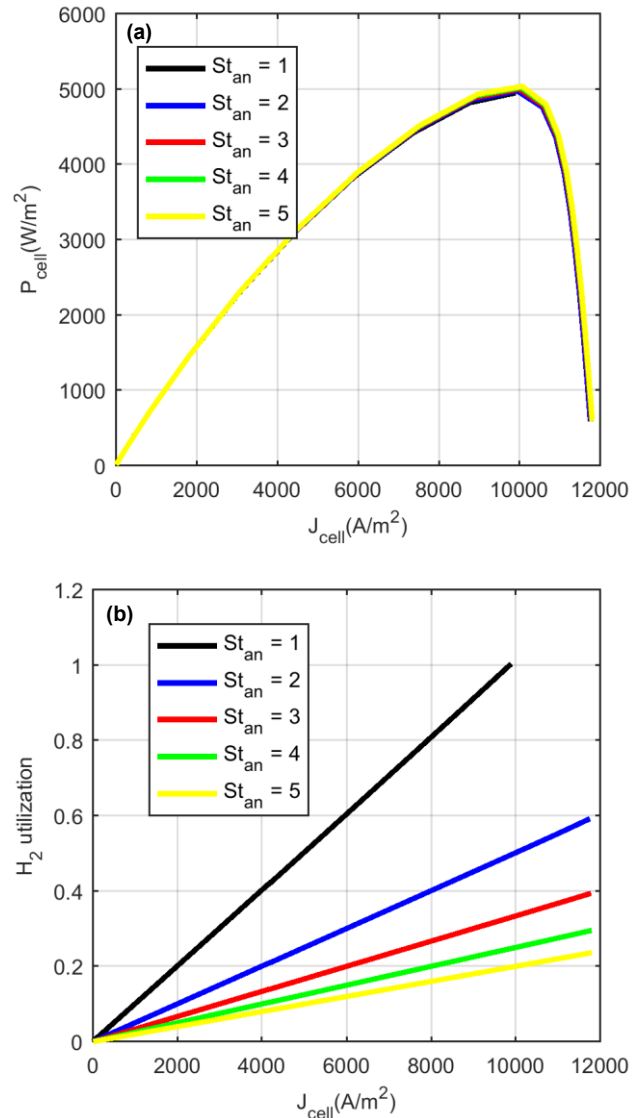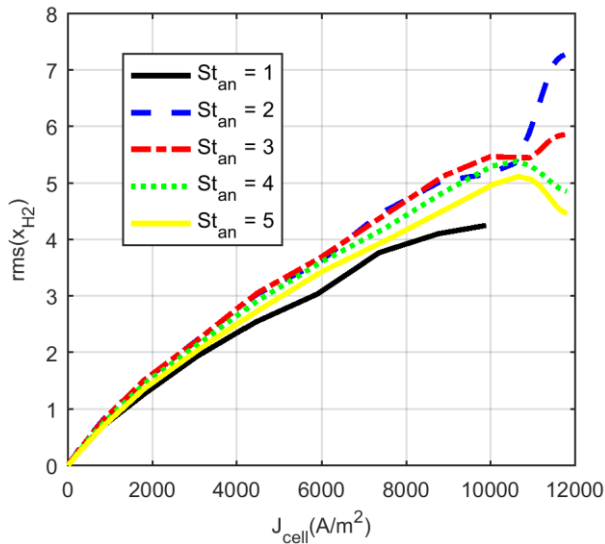

FIGURE 6: Effect of the anode stoichiometric ratio on: a) output power; b) hydrogen utilization; cathode stoichiometric ratio is fixed to 3

results in non-uniform hydrogen distribution in the active area. Hydrogen uniformity is examined by the root-mean-square (rms) of hydrogen mole fraction over the active area:

$$rms(\mathrm{x}_{H_2}) = \frac{\sqrt{\int \left(\mathrm{x}_{H_2} - \overline{\mathrm{x}}_{H_2} \right)^2 dA}}{\overline{\mathrm{x}}_{H_2} \, A_{active}} \qquad (34)$$

where $\overline{\mathrm{x}}_{H_2}$ is the mean of the hydrogen mole fraction in the active area. It is seen that hydrogen uniformity is almost the same for different anode stoichiometric ratios for the current density less than 10^4 A/m^2, as illustrated in Fig. 7. However, the hydrogen distribution gets more non-uniform for lower anode stoichiometric ratio in comparison to higher anode stoichio

7

FIGURE 7: Effect of the anode stoichiometric ratio on the hydrogen uniformity in the flow field; cathode stoichiometric ratio is fixed to 3

metric ratio for the current density higher than $10^4 A/m^2$. Since the stoichiometric ratios are defined with respect to $J_{cell}=10^4 A/m^2$, hydrogen utilization goes to zero at lower current densities and rms values for H_2 cannot be defined for higher values at $St_{an}=1$. For higher stoichiometric ratios, due to concentration losses in the cathode catalyst layer, cell potential goes to zero for higher current densities than $J_{cell}=1.2\times10^4 A/m^2$. Otherwise, hydrogen starvation is not an important issue that leads to this behavior.
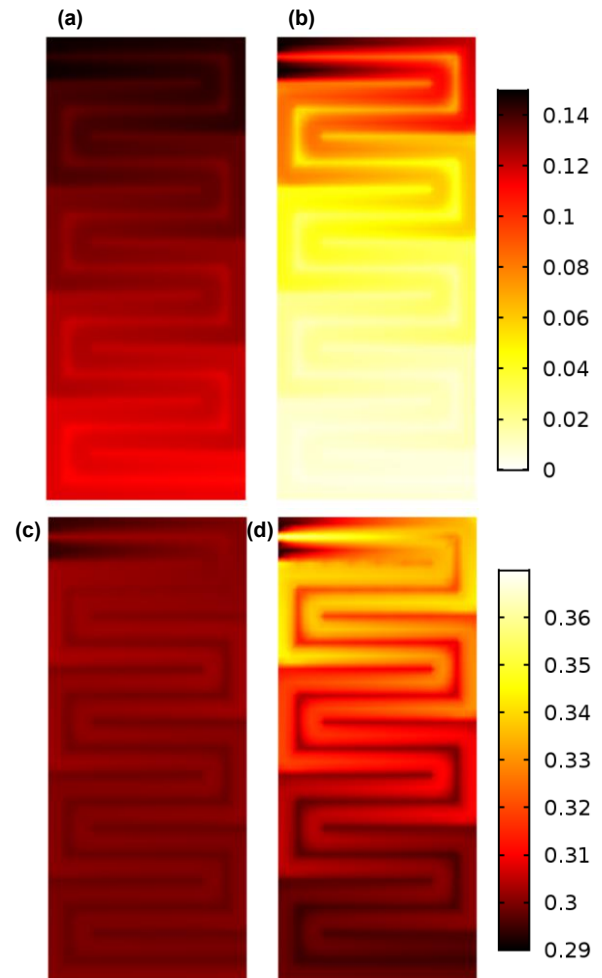
Figure 8a shows the oxygen distribution in the cathode active area for $St_{ca}=St_{an}=3$ and $J_{cell}=10^4 A/m^2$. Oxygen mole
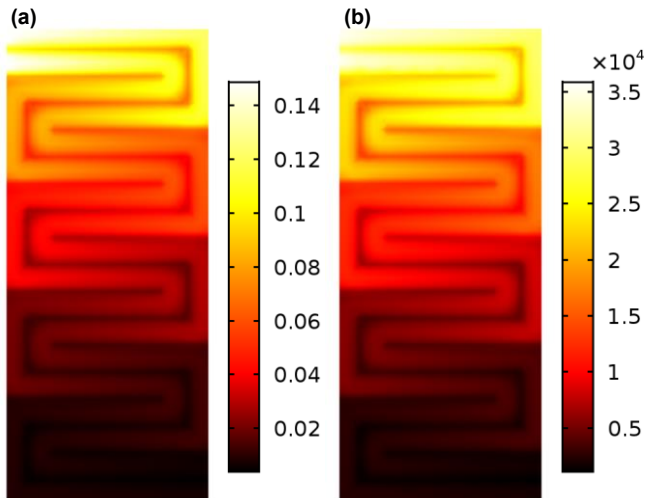
FIGURE 8: Oxygen (a) and current density (b) distribution for the stoichiometric ratios of 3 for the cathode and 3 for the anode side; average current density is fixed to $1.18\times10^4 A/m^2$

fraction drops to zero at the outlet which leads to local current density of zero at the outlet, as indicated in Fig. 8b. Therefore, the concentration loss is increased and stops the process for the stoichiometric ratio of 3 for the cathode side.

One of the goals of this model is a quick check of the species distribution in the anode and cathode channels that can be used to design flow fields for the cell. Species distribution in the active area obtained from the model is reasonable and consistent with the common trends reported in the literature. Figure 9 shows the effect of the current density on the oxygen and water vapor distribution in the cathode active area for the low and high current densities of 3×10^3 and $1.18\times10^4 A/m^2$, respectively. A uniform oxygen and water vapor distribution is observed for the low current density, Figs. 9a and 9c. However, for the higher current density oxygen starvation is seen at the end of the cathode active area, Fig. 9b, and higher water vapor due to higher reactions is observed around the inlet, Fig. 9d.

FIGURE 9: Oxygen distribution in the cathode active area for the current density of: a) $3\times10^3 A/m^2$, b) $11.8\times10^3 A/m^2$; water vapor distribution in the cathode active area for the current density of: c) $3\times10^3 A/m^2$, d) $11.8\times10^3 A/m^2$; the stoichiometric ratios of the anode and cathode sides are fixed to 3

5. CONCLUSION

A two-dimensional, in-plane, single-phase, and isothermal model of a single PEMFC has been developed. Channels and GDLs of both anode and cathode sides are considered. To evaluate the flow distribution in the channels and GDLs, Brinkman equations are used to include the fluid and stress transport at the void and solid boundaries of the channels and GDLs. Brinkman equations are coupled to the mass transfer, and reactions kinetic models. The through-the-plane direction is included in the model by applying resistance relations in that direction. A good agreement is obtained between polarization curves from the 2D model and the 3D model reported by Ye & Van Nguyen [18]. Effect of the anode and cathode stoichiometric ratios on the cell performance, hydrogen utilization, and species distribution in the flow field are investigated here and the work is underway to extend this study for the effects of other operating parameters such as temperature, pressure and the relative humidity by taking advantage of the efficacy of this approach. Furthermore, this approach is also suitable for design optimization of geometric variables of the flow fields. Results demonstrate that to sustain high output power, cathode stoichiometric ratio must be sufficiently greater than one. Moreover, reducing anode stoichiometric ratio results in higher hydrogen utilization. Two-dimensional in-plane modeling approach will be applied to a large cell to obtain an optimum design with uniform species in the flow field under high fuel utilization and ultra-low stoichiometry flow conditions.

ACKNOWLEDGMENTS

REFERENCES

[1] Larminie, J., & Dicks, A. (2003). Fuel Cell Systems Explained, 2nd edn Wiley. New York, USA.

[2] Wang, Y., Chen, K. S., Mishler, J., Cho, S. C., & Adroher, X. C. (2011). A review of polymer electrolyte membrane fuel cells: technology, applications, and needs on fundamental research. Applied Energy, 88(4), 981-1007.

[3] Al-Baghdadi, M. A. S. (2013). PEM Fuel Cells: Fundamentals, Modeling, and Applications. International Energy and Environment Foundation.

[4] Weber, A. Z., Borup, R. L., Darling, R. M., Das, P. K., Dursch, T. J., Gu, W., ... & Mukundan, R. (2014). A critical review of modeling transport phenomena in polymer-electrolyte fuel cells. Journal of The Electrochemical Socie-ty, 161(12), F1254-F1299.

[5] Karvonen, S., Hottinen, T., Saarinen, J., & Himanen, O. (2006). Modeling of flow field in polymer electrolyte membrane fuel cell. Journal of power sources, 161(2), 876-884.

[6] Rostami, L., Nejad, P. M. G., & Vatani, A. (2016). A numerical investigation of serpentine flow channel with different bend sizes in polymer electrolyte membrane fuel cells. Energy, 97, 400-410.

[7] Hu, G., Fan, J., Chen, S., Liu, Y., & Cen, K. (2004). Three-dimensional numerical analysis of proton exchange membrane fuel cells (PEMFCs) with conventional and interdigitated flow fields. Journal of Power Sources, 136(1), 1-9.

[8] Vazifeshenas, Y., Sedighi, K., & Shakeri, M. (2015). Numerical investigation of a novel compound flow-field for PEMFC performance improvement. International Journal of Hydrogen Energy, 40(43), 15032-15039.

[9] Vafai, K., & Tien, C. L. (1981). Boundary and inertia effects on flow and heat transfer in porous media. International Journal of Heat and Mass Transfer, 24(2), 195-203.

[10] Wang, Y., & Wang, C. Y. (2006). A nonisothermal, two-phase model for polymer electrolyte fuel cells. Journal of the electrochemical society, 153(6), A1193-A1200.

[11] Whitaker, S. (1986). Flow in porous media I: A theoretical derivation of Darcy's law. Transport in porous media, 1(1), 3-25.

[12] Brinkman, H. C. (1949). A calculation of the viscous force exerted by a flowing fluid on a dense swarm of particles. Applied Scientific Research, 1(1), 27-34.

[13] Berning, T., Lu, D. M., & Djilali, N. (2002). Three-dimensional computational analysis of transport phenomena in a PEM fuel cell. Journal of power sources, 106(1), 284-294.

[14] Liu, X. L., Tan, Y. W., Tao, W. Q., & He, Y. L. (2006). A hybrid model of cathode of PEM fuel cell using the interdigitated gas distributor. International journal of hydrogen energy, 31(3), 379-389.

[15] Shi, Z., & Wang, X. (2007, October). Comparison of Darcy's law, the Brinkman equation, the modified NS equation and the pure diffusion equation in PEM fuel cell modeling. In COMSOL Conference.

[16] Auriault, J. L. (2009). On the domain of validity of Brinkman's equation. Transport in porous media, 79(2), 215-223.

[17] Yu, L. H., & Wang, C. Y. (2013). Darcy-Brinkman Flow Through a Bumpy Channel. Transport in porous media, 97(3), 281-294.

[18] Ye, Q., & Van Nguyen, T. (2007). Three-dimensional simulation of liquid water distribution in a PEMFC with experimentally measured capillary functions. Journal of the Electrochemical Society, 154(12), B1242-B1251.

[19] Bear, J. (2013). Dynamics of fluids in porous media. Courier Corporation.

[20] Spaid, M. A., & Phelan Jr, F. R. (1997). Lattice Boltzmann methods for modeling microscale flow in fibrous porous media. Physics of fluids, 9(9), 2468-2474.

[21] Vasil'ev, A. (2009). From the Hele-Shaw experiment to integrable systems: a historical overview. Complex analysis and operator theory, 3(2), 551-585.

[22] Bird, R. B., Stewart, W. E., & Lightfoot, E. N. (2002). Transport Phenomena 2ndEd. John Wiley & Sons, New York, 63, b21.

[23] Petersen, E. E. (1958). Diffusion in a pore of varying cross section. AIChE Journal, 4(3), 343-345.

[24] Ge, S., Li, X., Yi, B., & Hsing, I. M. (2005). Absorption, de-sorption, and transport of water in polymer electrolyte membranes for fuel cells. Journal of the Electrochemical Society, 152(6), A1149-A1157.

[25] Xing, L., Liu, X., Alaje, T., Kumar, R., Mamlouk, M., & Scott, K. (2014). A two-phase flow and non-isothermal agglomerate model for a proton exchange membrane (PEM) fuel cell. Energy, 73, 618-634.

[26] Sonntag, R. E., Borgnakke, C., Van Wylen, G. J., & Van Wyk, S. (1998). Fundamentals of thermodynamics (Vol. 6). New York: Wiley.

[27] Barbir, F. (2005). Main cell components, materials properties and processes. PEM Fuel Cells: Theory and Practice, 73-113.

[28] Rizvandi, O. B., & Yesilyurt, S. (2016, July). Design of Anode Flow Channels and Headers for a Large PEMFC Operating at Ultra-Low Stoichiometric Flow Conditions at the Anode Exit. In ASME 2016 14th International Conference on Nanochannels, Microchannels, and Minichannels collocated with the ASME 2016 Heat Transfer Summer Conference and the ASME 2016 Fluids Engineering Division Summer Meeting (pp. V001T13A002-V001T13A002). American Society of Mechanical Engineers.